

Structural, Morphological and Physical Properties of TiH₂ Incorporated Hydroxyapatite

Nanthini Amirthalingam

Anna University Chennai

Sathishkumar Panchatcharam

Anna University Chennai

THENMUHIL Deivarajan (✉ thenmuhil@annauniv.edu)

Anna University Chennai <https://orcid.org/0000-0002-0809-6196>

Manohar Paramasivam

Anna University Chennai

Research Article

Keywords: Hydroxyapatite, Perovskite, Microstructures, Sintering, porosity

Posted Date: June 2nd, 2021

DOI: <https://doi.org/10.21203/rs.3.rs-577270/v1>

License: © ⓘ This work is licensed under a Creative Commons Attribution 4.0 International License.

[Read Full License](#)

Cover letter

May 30, 2021

Editorial Department of Journal of Advanced Ceramics
Tsinghua University Press
B605D, Xue Yan Building, Beijing 100084, China

Dear Editor of Journal of Advanced Ceramics

I am submitting a manuscript for consideration of publication in Journal of Advanced Ceramics. The manuscript is entitled “Structural, Morphological and physical properties of TiH₂ incorporated Hydroxyapatite”.

It has not been published elsewhere and that it has not been submitted simultaneously for publication elsewhere.

Titanium incorporated Hydroxyapatite preparation was endeavored using TiH₂. The hydroxyapatite (HAp) was obtained from wet chemical facile method and was mixed with TiH₂ (5 to 20%). The mixes were shaped by pressing and samples were sintered at different temperatures from 900°C to 1200°C. The experimental result from XRD clearly reveals that the product composition leads to TCP and CaTiO₃ major phases. SEM results showed that grain size increased at 1200°C with increase in wt % of TiH₂. The outcome of the sintering studies carried out shows that the maximum porosity was obtained at 5wt% of TiH₂ addition with the HAp at sintering temperatures of 900°C and 1000°C. The incidence of broad sintering reactions and phase dissociation of HAp leads to development of TCP–CaTiO₃ composites.

Thank you very much for your consideration.

Yours Sincerely,

Dr. Thenmuhil Deivarajan

Anna University

Chennai – 600 025

Tel.: 044 2235 9200

E-mail: thenmuhil@annauniv.edu

Structural, Morphological and physical properties of TiH₂ incorporated Hydroxyapatite

Nanthini Amirthalingam^a, Sathishkumar Panchatcharam^a, Thenmuhil Deivarajan^{a,*}, Manohar Paramasivam^a

^a Department of Ceramic Technology, Alagappa College of Technology, Anna University, Chennai 600 025.

Authors Email Id: nanthini2k@gmail.com, passathis@gmail.com, pmano@annauniv.edu

Corresponding Authors Email: *thenmuhil@annauniv.edu

Tel: 044 2235 9200.

Abstract

Titanium incorporated hydroxyapatite preparation was endeavored using TiH₂. Titanium has good mechanical properties, good biocompatibility and bioactivity. Titanium incorporated hydroxyapatite material prepared for orthopedic applications were reported to be better mechanical properties. Hydroxyapatite (HAp) was synthesized by wet chemical facile method and after calcination was mixed with TiH₂ (5 to 20%). The effect of sintering on phase formation, microstructure, density and porosity of Hap/TiH₂ was studied by sintering at temperatures from 900°C to 1200°C. The properties of the samples were characterized using X-ray diffraction technique (XRD), Scanning electron microscopy (SEM), Fourier transform spectroscopy (FT-IR), density and porosity. The results from studies showed the presence of β -tricalcium phosphate (β -TCP) and perovskite (CaTiO₃) as the major crystalline phases; while minor reaction products like α -TCP and TTCP were also recorded for samples with higher amount of TiH₂ irrespective of sintering temperatures. Morphology evaluation by SEM revealed the presence of CaTiO₃ needle

structure at temperature till 1000°C, above which it appeared hexagonal due to crystal growth. Functional groups, density and porosity were also studied.

Keywords: Hydroxyapatite; Perovskite; Microstructures; Sintering; porosity

1.Introduction

Hydroxyapatite (HAp) is composed of a network of calcium orthophosphates and is widely used in biomedical applications like orthopedics and dentistry as it is similar to the mineral component of bone and teeth. HAp is water-insoluble, biodegradable and bioactive since after some time it is partially resorbed and replaced by natural bone[1]. HAp has been used in various bone repair and replacement applications in the form of dense or porous blocks, granules, powders, coatings or as a mineral component in a polymer composite [2]. HAp can be synthesized by different routes such as solid-state reaction, sol-gel process, hydrothermal process, micro emulsion technique, precipitation process, biomimetic process, etc. Among these methods, chemical precipitation is the widely used method as it is economical and provides pure product.

Natural bone and teeth are porous materials which have porosity in micrometer range. Sponge bone has 50 to 90% porosity with pore diameter of roughly 1 μm [3, 4]. Even the Haversian canals in cortical bone contains 3 to 12% porosity [5]. In teeth, the open porosity of the dental tissue ranges between 1.11% and 3.08% of its volume [6]. In bone tissue engineering, a scaffolding material is utilized either to actuate the development of bone from the encompassing tissue or to go about as a bearer or template for implanted bone cells or agents [7].

Porous structures and rough surfaces are essential for encouraging bone ingrowth and osteointegration, which makes dense HAp less resorbable and osteoconductive compared to porous HAp for the healing/filling of osseous defects. For obtaining cell migration and transportation of nutrients and metabolic wastes, highly porous architecture with interconnected porous network is important [8,9].

Porous material can be prepared by sacrificial template process[10,11,13] gel casting of foams [12], powder metallurgy [14], freeze drying [15] etc. All these methods result in porous structure with different pore characteristics. General pore creating materials are naphthalene, hydrogen peroxide and other similar materials which are easily vaporizable. In this work, TiH_2 in various amounts is added to HAp and characterized to investigate its ability to act as pore former due to the presence of hydrogen group. Further, the incorporation of titanium ion with HAp to form composite is investigated.

Titanium and its alloys have been widely utilized as metallic implant materials because of the blend of advantageous properties like good mechanical properties, good biocompatibility and bioinertness. F.N. Oktar studied the mechanical properties of TiO_2 (5 to 10wt %) added to HAp with different sintering temperatures between 1000 and 1300°C [17].

Research was earlier done on sintered density and microstructure modifications on the usage of TiH_2 powders along with Ti. When TiH_2 powder was used as an alternative starting material to Ti metal powder in titanium sponge preparation, it gives the benefit of reduced cost in titanium powder metallurgy since TiH_2 is a transitional product in the hydrogenation - dehydrogenate (HDH) operation[18-19]. TiH_2 particles are most encouraging than the pure Ti

Particles because of the sintering behavior of TiH_2 [20]. Previously, TiH_2 powders were used to enhance the foaming process of Titanium scaffolds in orthopedic applications [21].

The decomposition of the hydride is belated when TiH_2 powder is pre-treated in atmospheric air condition at certain temperature [23]. The dehydrogenation of TiH_2 occurs in a two-step process given as $\text{TiH}_2 \rightarrow \text{TiH}_x \rightarrow \alpha\text{-Ti}$, where $0.7 < x < 1.1$ [24]. The coloration of TiH_2 powder is the easiest way to estimate the stage of oxidation during the dehydrogenation of TiH_2 . During heat treatment, the black powder turned to olive green at 400°C , purple at 450°C and blue between 500°C and 550°C [22].

The purpose of this novel work is to prepare composites with synthetic HAp and TiH_2 , and to analyze whether TiH_2 had functioned as a pore former or an additive or both. 5 – 20wt. % of TiH_2 was added to HAp and sintered at 900°C - 1200°C in pressureless sintering to study the effect of sintering temperature on phase formation, microstructure, functional group formation, density and porosity of samples with different TiH_2 content.

2. Materials and methods

2.1. Materials

Hydroxyapatite [$\text{Ca}_{10}(\text{PO}_4)_6(\text{OH})_2$] samples were prepared using calcium nitrate ($\text{Ca}(\text{NO}_3)_2 \cdot 4\text{H}_2\text{O}$), diammonium hydrogen phosphate ($(\text{NH}_4)_2\text{HPO}_4$), and ammonia, which were purchased from Merck. Commercial TiH_2 (325 mesh powder) was procured from Alfa Aesar.

2.2. Powder synthesis

The HAp powder was prepared by wet chemical precipitation method. Stoichiometric amount of $\text{Ca}(\text{NO}_3)_2 \cdot 4\text{H}_2\text{O}$ was gradually added into solution of $(\text{NH}_4)_2\text{HPO}_4$, with stirring. Ammonia was added drop wise into the mixed solution with vigorous stirring until pH reached a value of around 10 to 11, and was continued for 2 -3 hours to allow the reaction to take place towards completion. A white precipitate was obtained and was aged for 12 hours at room temperature. The obtained precipitate was filtered, washed with deionized water for 3-4 times and dried at 110°C for 24 hours. The dried lumps were crushed using an agate mortar and calcined at 700°C . The powder was confirmed as pure hydroxyapatite by matching the XRD pattern obtained (**Fig.1**) using D8 Advance (Bruker) analytical x-ray system with JCPDS file 09-0432.

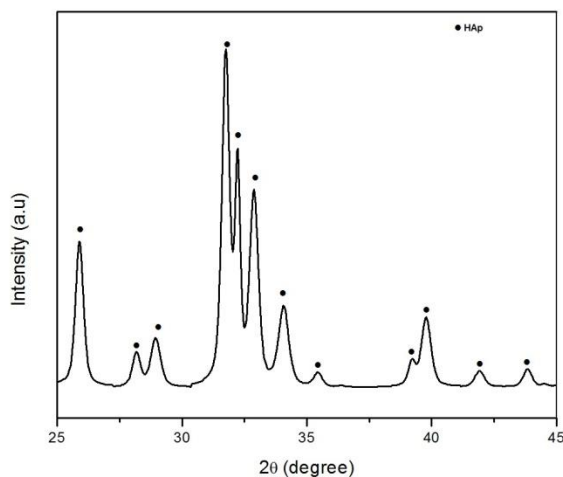


Fig.1. XRD pattern of pure HAp calcined at 700°C

2.3. Pellet Formation

TiH_2 was added in different weight percentages of 5, 10, 15 and 20 to HAp, and mixed with pestle and mortar for homogenous mixing. Pellets of 10mm diameter were prepared using

uniaxial press under 150 bars load. The as-mixed composite powders and pellets of HAp/TiH₂ were dried at 110°C for 24 hours and firing was done in a muffle furnace at temperatures of 900°C, 1000°C, 1100°C and 1200°C with 3°C per minute heating rate and 2 hours soaking at the maximum temperature.

2.4. Sample characterization

Phase analysis and lattice parameters of sintered HAp/TiH₂ powders were determined by X-ray diffraction (XRD) using Bruker D8 advance analytical x-ray system. The XRD patterns of the samples were obtained by using OriginPro software. An estimation of the crystallite size was obtained using the Debye-Scherrer equation (1)

$$D = \frac{K\lambda}{\beta \cos\theta} \dots\dots\dots(1)$$

where,

β is the peak width at half maximum intensity(FWHM) (in radians)

K is the Scherrer constant dependent on crystal habit (0.9)

λ is the wavelength of X-rays (1.5406Å for CuK _{α} radiation)

D is the crystallite size (nm)

θ is Bragg's diffraction angle(°)

The lattice constants of the HAp/TiH₂ powders were determined by the following relation(2)

$$\frac{1}{d^2} = \frac{4}{3} \left(\frac{h^2+k^2+l^2}{a^2} \right) + \frac{l^2}{c^2} \dots\dots\dots(2)$$

The volume of the hexagonal unit cell of the materials was calculated according to the formula,
 $V=0.866a^2c$ (3)

where, V is the volume of unit cell (nm³), a and c are the lattice constants.

Scanning electron microscopic (SEM) analysis (Quanta 200 FEG) was used for analyzing the size and morphology of sintered HAp/TiH₂ powders. FTIR (PerkinElmer) was performed to assess the functional groups and chemical composition of the sintered HAp/TiH₂ powders, for which the powders were mixed with KBr and pelletized, and spectra was obtained between 4000 – 400 cm⁻¹.

The density and porosity of the sintered HAp/TiH₂ pellets were tested by Archimede's principle with water as fluid and calculated using the formula (4) and (5) respectively

$$\text{Apparent porosity (\%)} \text{ is } \frac{S-D}{S-I} \times 100 \text{(4)}$$

$$\text{Apparent (bulk) density (g/cc)} \text{ is } \frac{D}{S-I} \text{(5)}$$

where, S is weight of the soaked piece (gm), D is weight of the dry piece (gm), I is weight of the immersed piece (gm).

3. Results and discussion

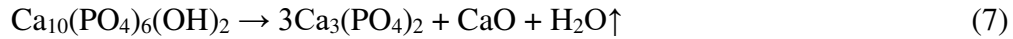
3.1. Structural characterization

The decomposition characteristics of HAp are reported variedly in literatures. It was reported that at sintering temperatures from 650°C to 1200°C, HAp decomposes into β-tricalcium phosphate [25]. The decomposition of HAp to Tri Calcium Phosphate (TCP –

$\text{Ca}_3(\text{PO}_4)_2$) and Tetra Calcium phosphate (TTCP – $\text{Ca}_4(\text{PO}_4)_2\text{O}$) occur at temperatures greater than 1200°C according to the reaction given in eq.(6) [26].



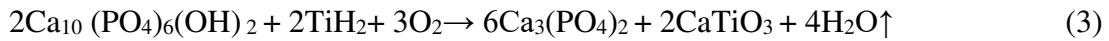
The following formula was proposed to account for the decomposition of HAp when it is sintered to higher temperature (1350°C) [27].



According to equations (6) and (7), both the decomposition and dehydroxylation reactions include water vapour as a by-product, and the rates at which these reactions continue depend on the moisture in the furnace atmosphere. Thus, the secondary phase formation during sintering could be controlled by controlling the sintering atmosphere. High amount of humidity present in sintering atmosphere has the tendency to delay decomposition rate by inhibiting the dehydration of OH^- group from the HAp matrix. This can be attained by controlling the partial pressure of the atmosphere, as the saturated moisture content in the atmosphere would suppress the by-product of water vapour between the reactions of both the dehydroxylation and decomposition [28]. In general, sintering at elevated temperatures tends to take the OH^- (hydroxide group) in the HAp matrix and concludes in the decomposition of HAp into α -TCP, β -TCP and TTCP [25, 29].

Fig.2 gives the X-ray spectra of the HAp/ TiH_2 sintered at different temperatures, and it reveals the presence of HAp, decomposition phases of HAp and a new phase relative to CaTiO_3 traces which indicates the interaction between HAp and TiH_2 . According to the phase compositions, it is obvious that CaTiO_3 is a product of reaction between TiO_2 and CaO , which is one of the decomposition products of HAp (according to Eq. (7)). CaTiO_3 was registered in the

XRD pattern of composite powders (irrespective of TiH₂ content) in Fig. 2, but there was no evidence of TiO₂, suggesting high thermodynamic tendency of TiH₂ to diffuse and then to react with HAp. However, the formation of CaTiO₃ indicates that the reaction between HAp and TiH₂ has taken place during thermal treatment. Hence, the interaction between TiH₂ and HAp at higher temperature (>900°C) is proposed as in equation (3).



Diffraction peaks from CaTiO₃ were observed from 900°C onwards, and its intensity was found to increase with increasing percentage of TiH₂ while that of apatite peaks decreased. The sharpness of CaTiO₃ peaks increased with the sintering temperature hinting on the increased crystallinity. The HAp decomposition phase formed at a particular temperature was found to be influenced by the TiH₂ content and the traces of pure HAp was found to remain undecomposed till 1200°C. The HAp decomposition phases were observed from 15wt% TiH₂ at 900°C, and 5wt% TiH₂ at 1000°C and the major phase was found to be β-TCP. Traces of α-TCP and TTCP formation at 900°C and 1000°C was found only on addition of 20wt% TiH₂.

Contrary to the above observations, α-TCP formation had initiated from 5wt% TiH₂ at 1100°C but the peaks became prominent only above 15wt% TiH₂. The other decomposition phase obtained with α-TCP was β-TCP. TTCP formation was observed from 15wt% TiH₂ at 1100°C. Samples sintered at 1200°C were observed to have CaTiO₃ and β-TCP as their major phases at various TiH₂ content. Additionally, minor peaks of α-TCP were found from 10wt% TiH₂. TTCP peaks was absent at 1200°C.

Fig.3, presents the crystallite size versus TiH₂ content at different sintering temperature ranging from 900 to 1200°C. The crystallite size was found to increase with increasing amount

of TiH_2 , and with increase in sintering temperature. The increase in the crystallite size with increase in the sintering temperature can be attributed to crystal growth and densification. The lattice constants of HAp/ TiH_2 was evaluated for all the sintered HAp/ TiH_2 samples and are listed in Table 1 & 2. These values were found not to vary appreciably as a function of TiH_2 content and heat treatment temperature.

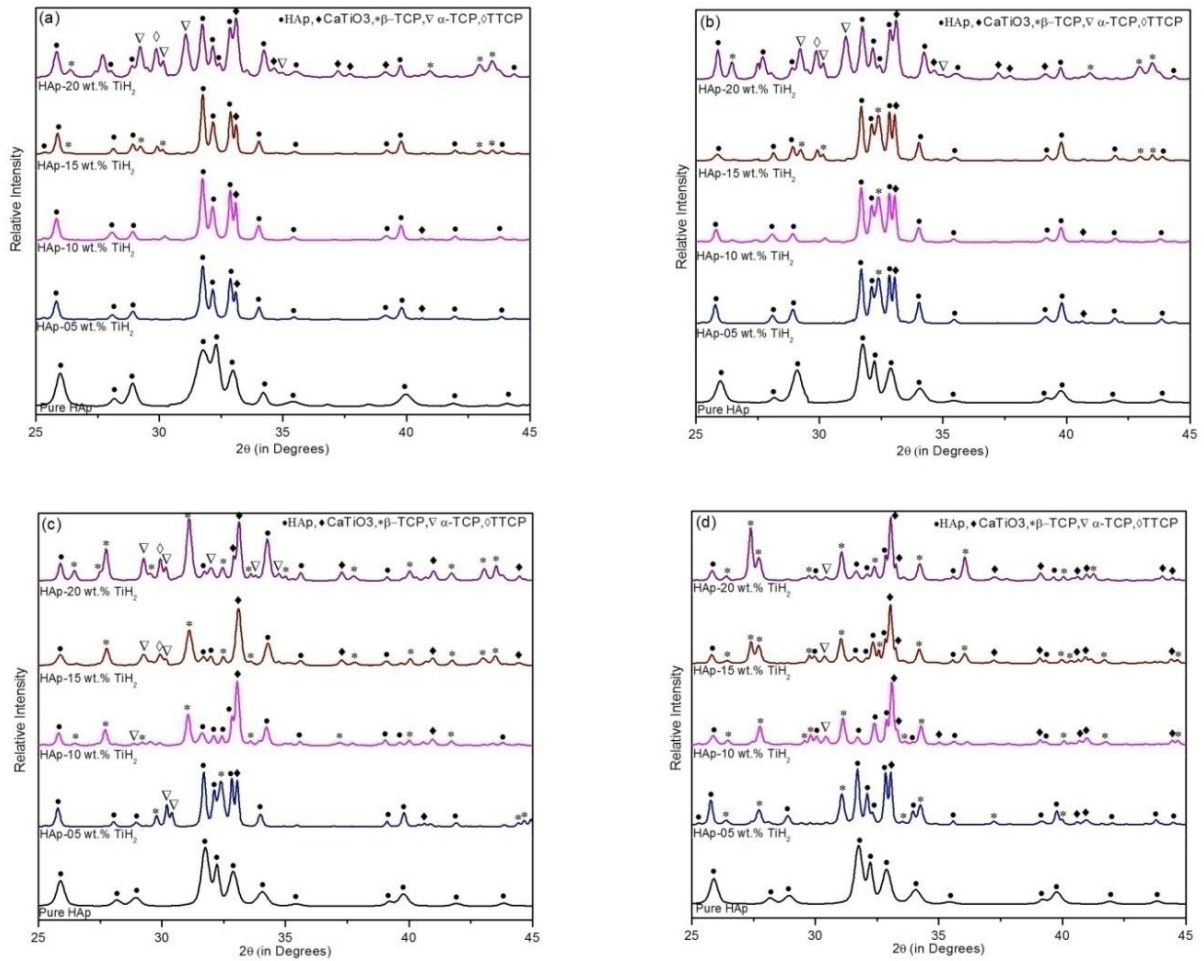


Fig.2. XRD peaks obtained after sintering at temperatures of (a) 900°C (b) 1000°C (c) 1100°C and (d) 1200°C for HAp with different TiH_2 contents

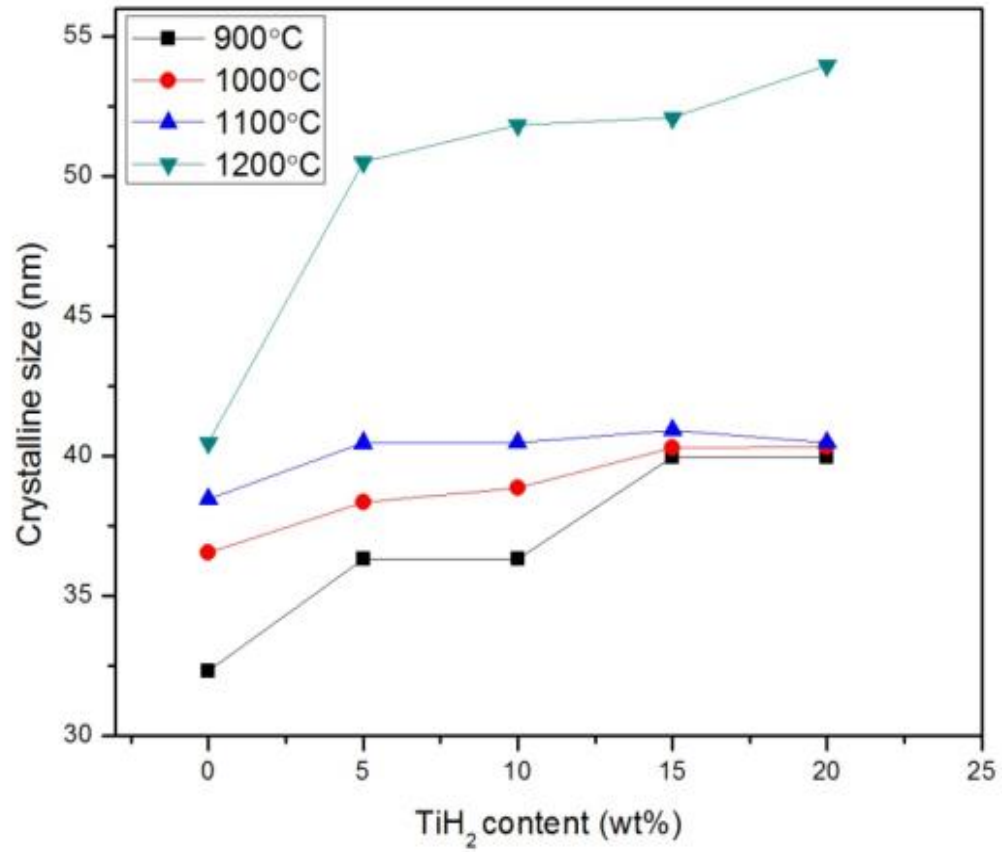


Fig.3. Plot of the crystallite size vs. TiH₂ content at various temperatures

Table 1.

Crystallite size, Lattice parameter and Cell volume of HAp with different TiH₂ content at 900°C and 1000°C

Temperature →	900°C				1000°C			
Sample Name↓	Ds (nm)	a(Å)	c(Å)	V(Å ³)	Ds (nm)	a(Å)	c(Å)	V(Å ³)
HAp-05wt.% TiH ₂	36.3391	9.426	6.889	530.1	38.5390	9.428	6.889	530.2
HAp-10wt.% TiH ₂	36.3395	9.422	6.879	528.9	38.6127	9.425	6.878	529.1
HAp-15wt.% TiH ₂	39.9770	9.425	6.888	529.9	39.9956	9.423	6.892	529.9
HAp-20wt.% TiH ₂	39.9743	9.443	6.877	531.0	39.9923	9.433	6.890	530.9

Table 2.

Crystallite size, Lattice parameter and Cell volume of HAp with different TiH₂ content at 1100°C and 1200°C

Temperature →	1100°C				1200°C			
Sample Name↓	Ds (nm)	a(Å)	c(Å)	V(Å ³)	Ds (nm)	a(Å)	c(Å)	V(Å ³)
HAp-05wt.% TiH ₂	40.4836	9.419	6.880	528.6	50.5138	9.429	6.888	530.4
HAp-10wt.% TiH ₂	40.4860	9.419	6.881	528.7	51.8497	9.429	6.877	529.5
HAp-15wt.% TiH ₂	40.9410	9.438	6.879	530.8	52.0920	9.423	6.893	530.0
HAp-20wt.% TiH ₂	40.4917	9.426	6.880	529.4	53.9825	9.419	6.879	528.6

3.2. Morphological Characterization

Small diameter elongated particles having needle like appearance, were observed on samples sintered at 900°C & 1000°C irrespective the amount of TiH₂ added. These particles can be confirmed to be CaTiO₃ from the XRD patterns (Fig. 2. a & b) for a particular percentage of TiH₂ added, the distribution of CaTiO₃ particles was more at 1000°C when compared to that at 900°C. As the sintering temperature increased to 1100°C and 1200°C, these smaller particles became coarser and elongated due to enhanced crystal growth of CaTiO₃ which can be confirmed with the sharpening of XRD peaks as observed from Fig. 2.c&d. Average grain size was increased upto 1.468µm and 1.890µm at the corresponding sintering temperature of 1100°C and 1200°C.

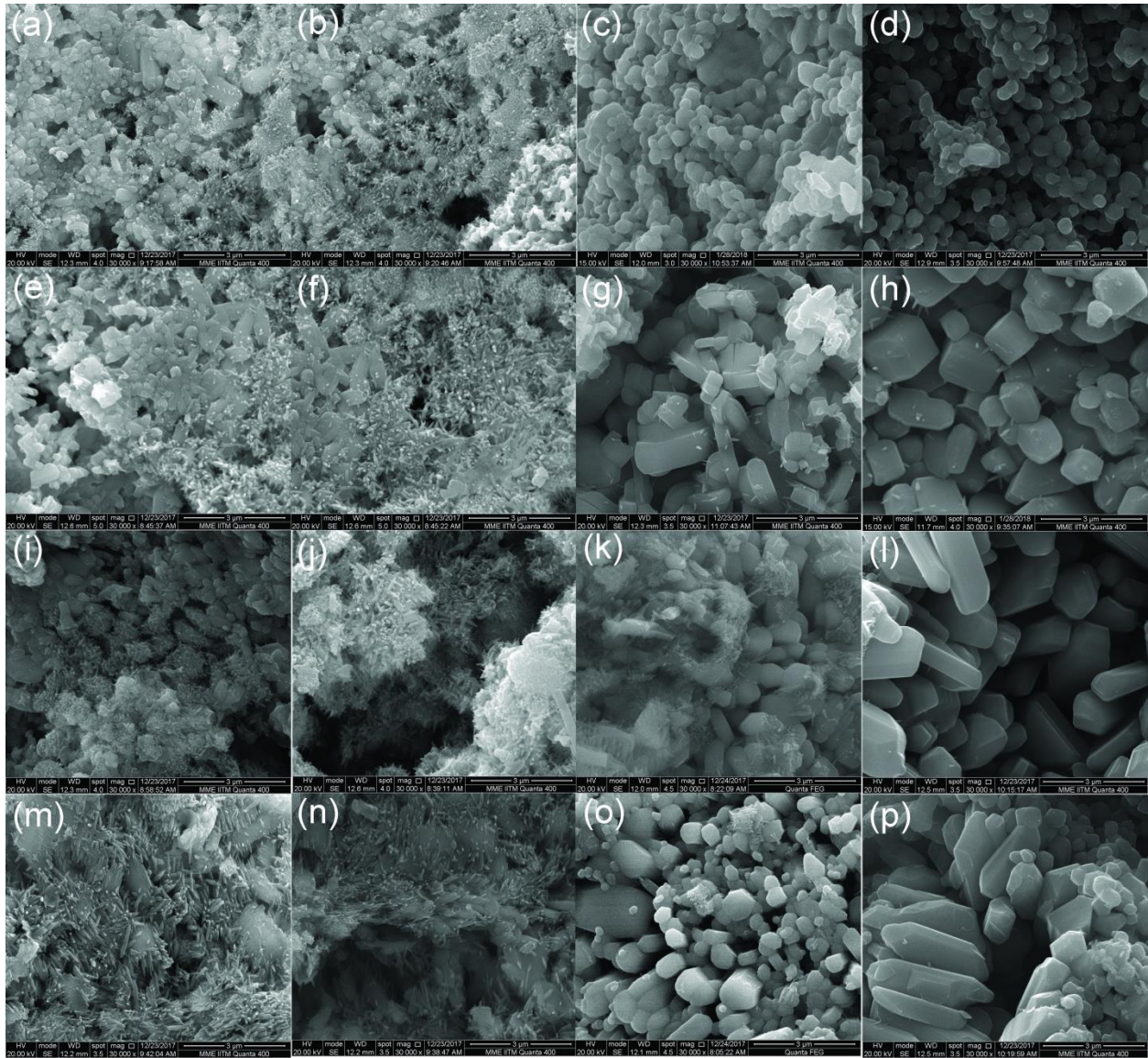


Fig.4. SEM micrographs showing different morphological characteristics: (a), (e), (i) and (m) HAp-5%,10%,15% and 20% TiH₂ sintered at 900°C; (b) (f), (j) and (n) HAp-5%,10%,15% and 20% TiH₂ sintered at 1000°C; (c) (g), (k) and (o) HAp-5%,10%,15% and 20% TiH₂ sintered at 1100°C, (d) (h), (l) and (p) HAp-5%,10%,15% and 20% TiH₂ sintered at 1200°C.

3.3. FTIR Analysis

The FTIR spectrum of the samples heat treated at 900°C, 1000°C, 1100°C and 1200°C without and with different percentages of TiH₂ are shown in Fig.5. Most bands characterize the phosphate group of HAp, especially at 570 cm⁻¹, 605 cm⁻¹, 1038-1049 cm⁻¹ and 1119 - 1120cm⁻¹ as mentioned in Table.3. A sharp peak with weak intensity corresponding to OH⁻ stretching vibration band is observed at 3571 cm⁻¹ in pure HAp sample. This band is totally absent at higher TiH₂ content or at higher temperature due to the dehydroxylation as a result of HAp decomposition . Weak bonds at 944cm⁻¹ and 550 cm⁻¹ related to the secondary β-TCP phase in HAp were observed in all HAp/TiH₂ samples. The peak at 605 cm⁻¹ are assigned to the asymmetric deformation of the PO₄³⁻ ions (ν₁). The peaks at 944 cm⁻¹and 962 cm⁻¹ are relative to the symmetric stretching of the PO₄³⁻ ions (ν₃) and the peaks at 1038 – 1090 cm⁻¹ and 1119 - 1120 cm⁻¹ are relative to the asymmetric stretching of the PO₄³⁻ ions (ν₃). Furthermore, the relative intensity between the peaks at ~478 cm⁻¹ and that at ~470 cm⁻¹ reflects the degree of the dehydroxylation. The peak at 478 cm⁻¹ is slightly stronger than the peak at 470 cm⁻¹. In addition to the above mentioned peaks, few other peaks are also detected at around 2350 and 2923 cm⁻¹ which are due to KBr used for sample preparation [30].

Table 3.

Observed FTIR band positions and their assignment.

Sample Name →	Pure HAp	HAp-05wt.% TiH ₂	HAp-10wt.% TiH ₂	HAp-15wt.% TiH ₂	HAp-20wt.% TiH ₂	Assignment	References
Temperature ↓	Vibrational frequency (cm ⁻¹)						
	470.59	-	-	-	-	ν ₂ bending mode of P-	[31]

						O mode	
900°C	570.95	570.95	570.95	570.95	570.95	O-P-O bending	[32]
	601.74	601.84	601.84	601.84	601.84	ν_4 bending mode of O-P-O mode	[31,32]
	632.60	632.67	632.67	632.67	632.67	ν_4 (PO_4^{3-})	[34]
	-	962.52	962.52	962.52	962.52	ν_3 (PO_4^{3-})	[31]
	1049.19	1043.53	1043.53	1043.53	1043.53	ν_3 (PO_4^{3-})	[34]
	2360.69	2360.97	2360.97	2360.97	2381.22	-	[30]
	3571.90	3571.36	3571.36	3571.36	3571.36	The vibrational of OH^-	[34,35]
1000°C	~478.31	-	-	-	-	Dehydroxylation	[35]
	570.88	567.09	567.09	567.09	567.09	ν_4 (PO_4^{3-})	[34]
	606.6	606.6	606.6	606.6	606.6	ν_4 (PO_4^{3-})	[34]
	-	944.20	944.20	944.20	944.20	ν_2 (PO_4^{3-})	[33]
	1049.19	1041.61	1041.61	1041.61	1041.61	ν_3 (PO_4^{3-})	[34]
	-	1120.69	1120.69	1120.69	1120.69	ν_3 (PO_4^{3-})	[33]
	2360.69	2363.86	2363.86	2363.86	2363.86	-	[30]
1100°C	478.31	-	-	-	-	Dehydroxylation	[35]
	570.88	550.70	550.70	550.70	550.70	ν_4 (PO_4^{3-})	[34]
	605.67	605.67	605.67	605.67	605.67	ν_1 (PO_4^{3-})	[33]
	-	944.19	944.19	944.19	944.19	ν_2 (PO_4^{3-})	[33]
	1049.19	1041.60	1041.60	1041.60	1041.60	ν_3 (PO_4^{3-})	[34]
	-	1119.72	1119.72	1119.72	1119.72	ν_3 (PO_4^{3-})	[33]
	2360.69	2360	2360	2360	2360	-	[30]
1200°C	478.31	-	-	-	-	Dehydroxylation	[35]
	563.17	550.70	550.70	550.70	550.70	ν_4 (PO_4^{3-})	[34]
	-	604.70	603.74	603.74	602.78	ν_1 (PO_4^{3-})	[33]
	-	944.19	944.19	944.19	944.19	ν_2 (PO_4^{3-})	[33]
	1049.19	1042.56	1042.56	1042.56	1042.56	ν_3 (PO_4^{3-})	[34]
	2360.69	2360	2360	2360	2360	-	[30]

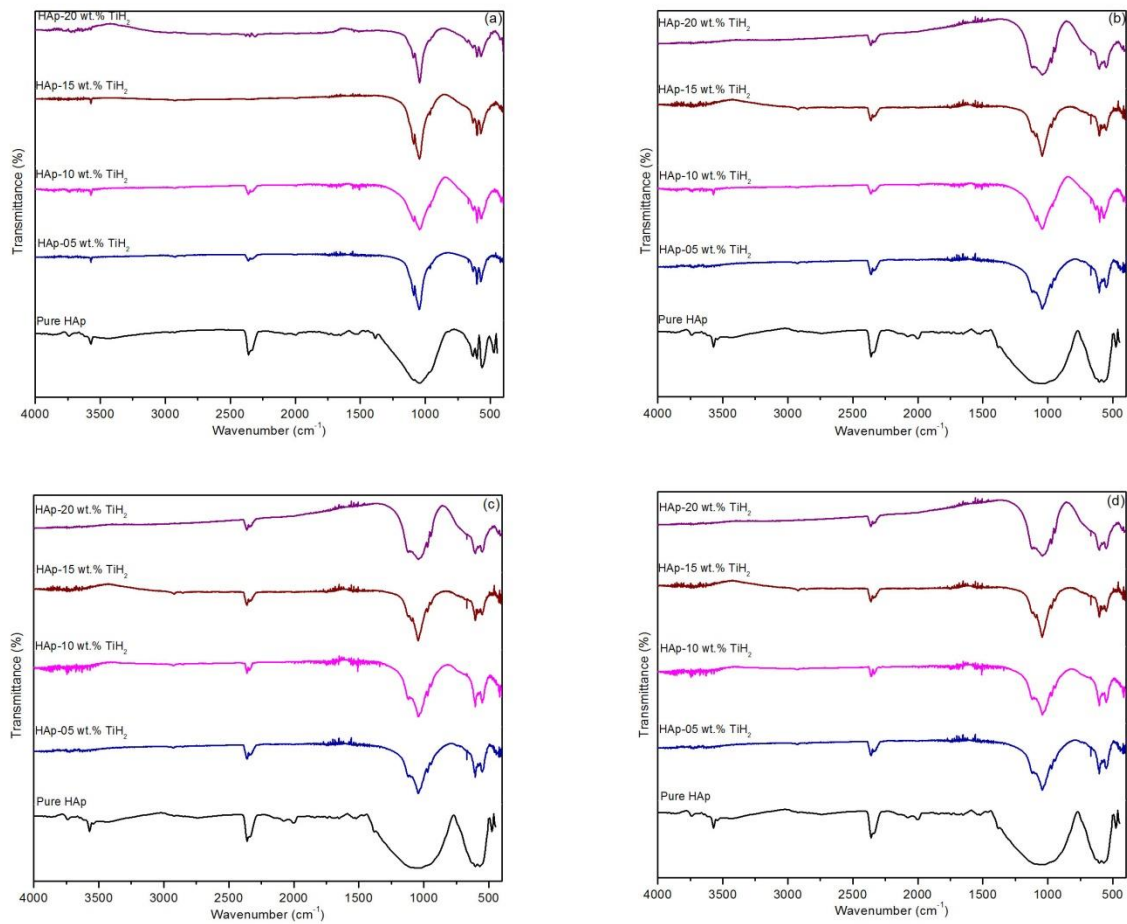


Fig.5. FT-IR spectra obtained after sintering at (a) 900°C, (b) 1000°C, (c) 1100°C and (d) 1200°C from various HAp-TiH₂ composites

3.4. Density and Porosity

Density of HAp/TiH₂ composite was found to increase with increase in TiH₂ weight percentage at 900°C and 1000°C. Density values decreased above 1000°C due to the decomposition of HAp, due to which the porosity of the composite has increased. As can be observed from the SEM images (Fig. 4) of HAp/TiH₂ samples heat treated at 900°C and 1000°C, formation of CaTiO₃ needle structures have filled the void spaces resulting in increased density. Above 1000°C, CaTiO₃ crystals were observed to grow proportionately with increasing

TiH₂ content and temperature. This leads to more open structure leading to decrease in density with increase in TiH₂ content at 1100°C and 1200°C. Corresponding inverse correlation for porosity was observed in all samples.

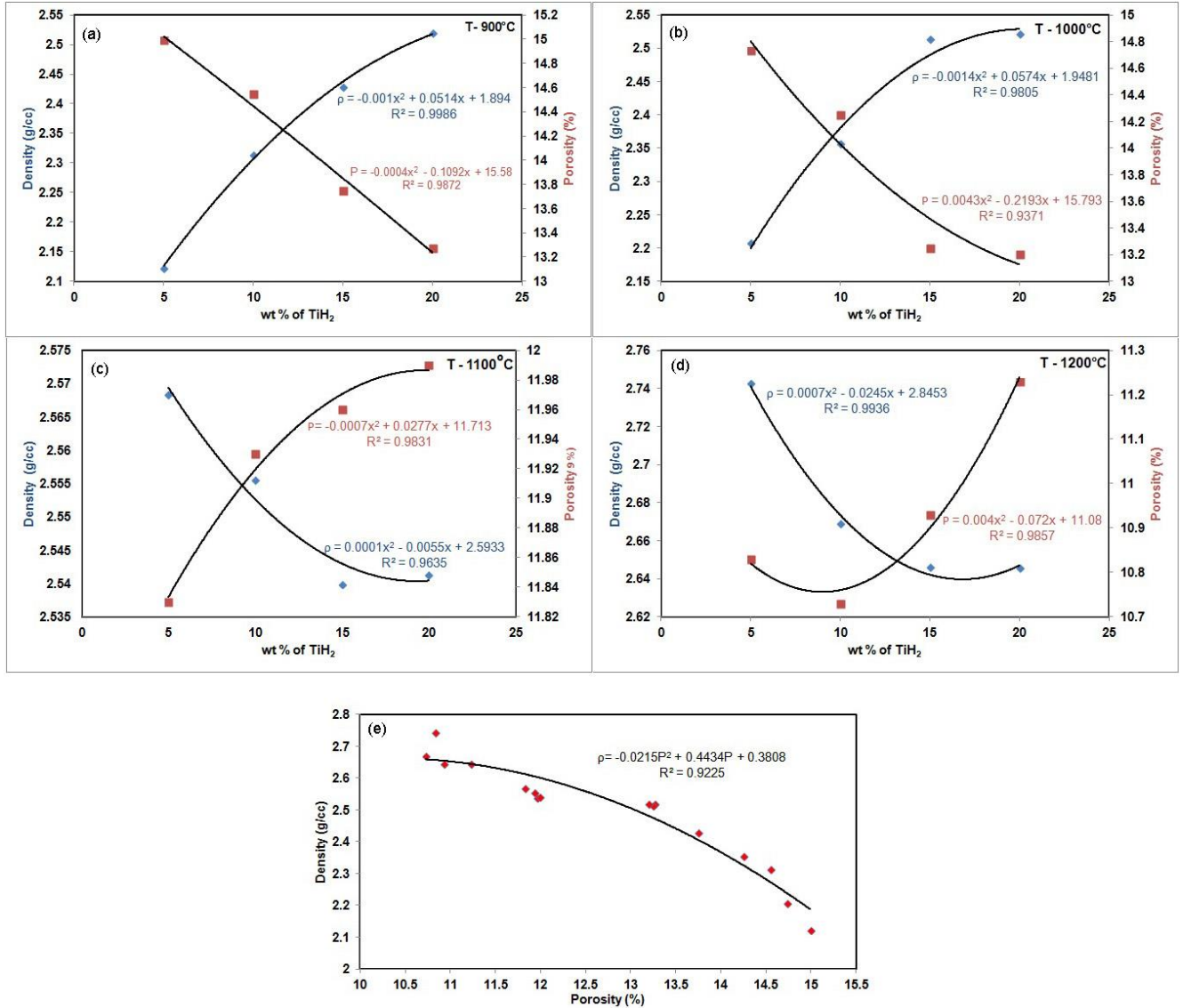


Fig.6. Density and porosity graph of HAp with different weight percentages of TiH₂ (a) sintered at 900°C (b) sintered at 1000°C (c) sintered at 1100°C(d) sintered at 1200°C(e) Overall graph of density vs porosity.

Fig.6.e. shows the overall graph for the density and porosity values, and shows that increase in density decreases the porosity of sample. The correlation co-efficient calculated from the graph drawn between the overall density and porosity was 0.9225.

Conclusions

Hydroxyapatite was prepared by precipitation method and powders of hydroxyapatite with different TiH₂ percentage were sintered in air atmosphere at the range of 900-1200°C for 2 h for simultaneously developing pore in the HAp and incorporate it with Titania. The experimental result from XRD clearly reveals that the product composition leads to TCP and CaTiO₃ major phases. SEM results showed that grain size increased at 1200°C with increase in wt % of TiH₂. The outcome of the sintering studies carried out shows that the maximum porosity was obtained at 5wt% of TiH₂ addition to HAp at sintering temperatures of 900°C and 1000°C. The incidence of broad sintering reactions and phase dissociation of HAp leads to development of TCP–CaTiO₃ composites. The mechanical properties and bioactivity of the samples will be studied in future.

References

- [1] Osborn JF, Newsley H. The material science of calcium phosphate ceramics. *Biomaterials* 1980, **1**: 108-11. [https://doi.org/10.1016/0142-9612\(80\)90009-5](https://doi.org/10.1016/0142-9612(80)90009-5).
- [2] Bonfield W, Grynblas MD, Tully AE, Bowman J, Abram J. Hydroxyapatite Reinforced Polyethylene — A Mechanically Compatible Implant Material for Bone-Replacement, *Biomaterials* 1981, **2** : 185–186. [http://doi.org/10.1016/0142-9612\(81\)90050-8](http://doi.org/10.1016/0142-9612(81)90050-8)
- [3] Boqing Zhang, Xuan Pei, Ping Song Huan Sun, Huiyong Li, Yujing Fan, Qing Jiang, Changachun Zhou, Xingdong Zhang. Porous bioceramics produced by inkjet 3D printing: Effect of printing ink formulation on the ceramic macro and micro porous architectures control. *Compos Part B* 2018, **155** : 112 – 121. <http://doi.org/10.1016/j.compositesb.2018.08.047>
- [4]. Keaveny TM, Morgan EF, Niebur GL, Yeh OC. Biomechanics of trabecular bone. *Annu. Rev. Biomed. Eng.* 2001, **3**: 307-333. <http://doi.org/10.1146/annurev.bioeng.3.1.307>.

- [5] Cooper DM, Matyas JR, Katzenberg MA, Hallgrímsson B. Comparison of microcomputed tomographic and microradiographic measurements of cortical bone porosity. *Calcif. Tissue Int.* 2004, **74**: 437-447. <http://doi.org/10.1007/s00223-003-0071-z>.
- [6] Figueiredo de MM, Neto Ferreira RA, Grossi PA, de Andrade RM. Measurement of thermophysical properties of human dentin: effect of open porosity. *J. Dent.* 2008, **36**: 588-594. <http://doi.org/10.1016/j.jdent.2008.04.006>.
- [7] HassnaRehmanRamay, Miqin Zhang. Preparation of porous hydroxyapatite scaffolds by combination of the gel-casting and polymer sponge methods, *Biomaterials* 2003, **24**: 3293–3302. [http://doi.org/10.1016/S0142-9612\(03\)00171-6](http://doi.org/10.1016/S0142-9612(03)00171-6).
- [8] Maria GraziaRauci , Vincenzo Guarino, Luigi Ambrosio. Hybrid composite scaffolds prepared by sol–gel method for bone regeneration, *Compos Sci and Tech* 2010, **70**: 1861–1868. <http://doi.org/10.1016/j.compscitech.2010.05.030>.
- [9] Gang Chen, Ning Chen, Qi Wang. Fabrication and properties of poly(vinyl alcohol)/ β -tricalcium phosphate composite scaffolds via fused deposition modeling for bone tissue engineering, *Compos Sci and Tech* 2019, **172**: 17–28. <http://doi.org/10.1016/j.compscitech.2019.01.004>.
- [10] Hench LL , Wilson J. *An Introduction to Bioceramics*, World Scientific Publishing Co. Ltd., 1993. <http://doi.org/10.1142/p884>.
- [11] Chunli Wang, Hongjie Chen, Xiangdong Zhu, Zhanwen Xiao, Kai Zhang, Xingdong Zhang. An improved polymeric sponge replication method for biomedical porous titanium scaffolds, *Mat Sci and Engg C Volume* 2017, **70**: 1192-1199. <http://doi.org/10.1016/j.msec.2016.03.037>.
- [12] Sepulveda P, Binner JG, Rogero SO, Higa OZ, Bressiani JC. Production of porous hydroxyapatite by gel-casting of foams and cytotoxic evaluation, *J of Biomed Mat Res* 2000, **50**: 27–34. [https://doi.org/10.1002/\(SICI\)1097-4636\(200004\)50:1<27::AID-JBM5>3.0.CO;2-6](https://doi.org/10.1002/(SICI)1097-4636(200004)50:1<27::AID-JBM5>3.0.CO;2-6)
- [13] Rodríguez-Lorenzo LM, Vallet-Regi M, Ferreira JMF. Fabrication of porous hydroxyapatite bodies by a new direct consolidation method: starch consolidation, *J of Biomed Mat Res* 2002, **60**: 232–240. <http://doi.org/10.1002/jbm.10036>.
- [14] Man-Tik Choy, Chak-Yin Tang, Ling Chen, Wing – Cheung Law, Chi-Pong Tsui, William Weijia Lu. Microwave assisted – in situ synthesis of porous titanium/calcium phosphate composites and their in vitro apatite – forming capability, *Compos Part B* 2015, **50** – 57. <http://doi.org/10.1016/j.compositesb.2015.08.046>
- [15] Nejati E, Mirzadeh H, Zandi M. Synthesis and characterization of nano-Hydroxyapatite rods/Poly(L- lactide acid) composite scaffolds for bone tissue engineering, *Compos part A* 2008, **39**: 1589 – 1596. <https://doi.org/10.1016/j.compositesa.2008.05.018>
- [16] Oktar FN. Hydroxyapatite–TiO₂ composites, *Materials Letters* 2006, **60**: 2207–2210. <http://doi.org/10.1016/j.matlet.2005.12.099>

- [17] Egorov AA, Smirnov VV, Shvorneva LI, Kutsev SV, Barinov SM. High Temperature Hydroxyapatite–Titanium Interaction, *Inorganic Matl.* 2010, **46**: 68–171. <http://doi.org/10.1134/S0020168510020147>
- [18] Ivasishin O, Moxson V, Qian M, Froes H. Low-Cost Titanium Hydride Powder Metallurgy, *Titanium Powder Metallurgy: Science, Technology and Applications*, Q. Ma and F.H. Froes, Ed., Butterworth- Heinemann, London 2015, 117–148. <https://doi.org/10.1016/B978-0-12-800054-0.00008-3>.
- [19] Wang CM, Pan L, Zhang YN, Xiao SF, Chen YG. Deoxidization mechanism of hydrogen in TiH₂ dehydrogenation process, *Int J Hyd Eng* 2016, **41**: 14836-14841. <https://doi.org/10.1016/j.ijhydene.2016.05.155>
- [20] Fumio Watari, Atsuro Yokoyama, Mamoru Omori, Toshio Hirai, Hideomi Kondo, MotohiroUo, Takao Kawasaki. Biocompatibility of materials and development to functionally graded implant for bio-medical application, *Compos Sci and Tech* 2004, **64**: 893–908. <https://doi.org/10.1016/j.compscitech.2003.09.005>.
- [21] Shuilin Wu, Xiangmei Liu, K.W.K. Yenung, Tao Hu, Zushun Xu, Jonathan C. Y. Chung, Paul K. Chu. Hydrogen release from titanium hydride in foaming of orthopedic NiTi scaffolds, *Actabiomaterialia* 2011, **7**: 1387-1397. <https://doi.org/10.1016/j.actbio.2010.10.008>
- [22] Kennedy AR .The effect of TiH₂heat treatment on gas release and foaming in Al–TiH₂ preforms. *Scr Mater* 2002, **47**: 763. [https://doi.org/10.1016/S1359-6462\(02\)00281-6](https://doi.org/10.1016/S1359-6462(02)00281-6).
- [23] Liu H, He P, Feng JC, Cao J. Kinetic study on non isothermal dehydrogenation of TiH₂ powders. *Int J Hyd Eng* 2009, **34**:3018. <https://doi.org/10.1016/j.ijhydene.2009.01.095>.
- [24] Bhosle V, Baburaj EG, Miranova M, Salama K. Dehydrogenation of TiH₂. *Mater SciEng A-Struct Mater Prop Microstruct Process* 2003, 356:190. [https://doi.org/10.1016/S0921-5093\(03\)00117-5](https://doi.org/10.1016/S0921-5093(03)00117-5).
- [25] Wei-Jen Shih, Jian-Wen Wang, Moo-Chin Wang, Min-Hsiung Hon. A study on the phase transformation of the nanosized hydroxyapatite synthesized by hydrolysis using in situ high temperature x-ray diffraction, *Mater Sci Engg C* 2006, **26**: 1434 – 1438. <https://doi.org/10.1016/j.msec.2005.08.005>
- [26] Chiba A, Kimura S, Raghukandan K, Morizono Y. Effect of alumina addition on hydroxyapatite biocomposites fabricated by underwater-shock compaction, *Mat Sci Engg A*, 2003, **350**: 179/183. [https://doi.org/10.1016/S0921-5093\(02\)00718-9](https://doi.org/10.1016/S0921-5093(02)00718-9).
- [27] jiming Z, Zhang C, Xingdong Z, Jiyong S, de Groot K. High temperature characteristics of synthetic hydroxyapatite. *J Mater Sci Mater Med* 1993, **4**: 83-5. <https://doi.org/10.1007/BF00122983>.
- [28] Ramesh S, Tan CY, Yeo WH, Tolouei R, Amiriyani M, Sopyan I, Teng WD. Effects of bismuth oxide on the sinterability of hydroxyapatite, *Ceram Intl* 2011, **37**: 599–606. <https://doi.org/10.1016/j.ceramint.2010.09.041>

- [29] Satoshi Kobayashi, Wataru Kawai. Development of carbon nanofiber reinforced hydroxyapatite with enhanced mechanical properties, *Compos Part A* 2007, **38**: 114–123. <https://doi.org/10.1016/j.compositesa.2006.01.006>
- [30] ShekharNath, Rajesh Tripathi, BikramjitBasu. Understanding phase stability, microstructure development and biocompatibility in calcium phosphate–titania composites, synthesized from hydroxyapatite and titanium powder mix, *Mater Sci and Engg C* 2009, **29**: 97–107. <https://doi.org/10.1016/j.msec.2008.05.019>.
- [31] Ana Janković, SanjaEraković, MiodragMitrić, Ivana Z. Matic, ZoricaD.Juranić, Gary C.P.Tsui, Chak-yinTang, VesnaMišković-Stanković, KyongYop Rhee, Soo Jin Park. Bioactive hydroxyapatite/graphene composite coating and its corrosion stability in simulated body fluid. *J. All. Com.* 2015, **624**: 148–157. <https://doi.org/10.1016/j.jallcom.2014.11.078>.
- [32] Ashok M, MeenakshiSundaram N, Narayana Kalkura S. Crystallization of hydroxyapatite at physiological temperature. *Mat. Lett.* 2003, **57**: 2066–2070. [http://doi.org/10.1016/S0167-577X\(02\)01140-0](http://doi.org/10.1016/S0167-577X(02)01140-0).
- [33] IbticemAyadi, Foued Ben Ayed. Sintering and the mechanical properties of the tricalciumphosphate–titaniacomposites, *j of the mech behav of biomed matls* 2015, **49**: 129–140. <https://doi.org/10.1016/j.jmbbm.2015.05.001>.
- [34] Rehman I, Bonfield W. Characterization of hydroxyapatite and carbonated apatite by photo acoustic FTIR spectroscopy, *J of Mater sci : Mater in Med* 1997, **8**: 1 –4. <https://doi.org/10.1023/A:1018570213546>
- [35] Hezhou Ye Æ Xing Yang Liu Æ Hanping Hong. Characterization of sintered titanium/hydroxyapatite biocomposite using FTIR spectroscopy, *J Mater Sci: Mater Med* 2009, **20**: 843–850. <https://doi.org/10.1007/s10856-008-3647-3>

Figures

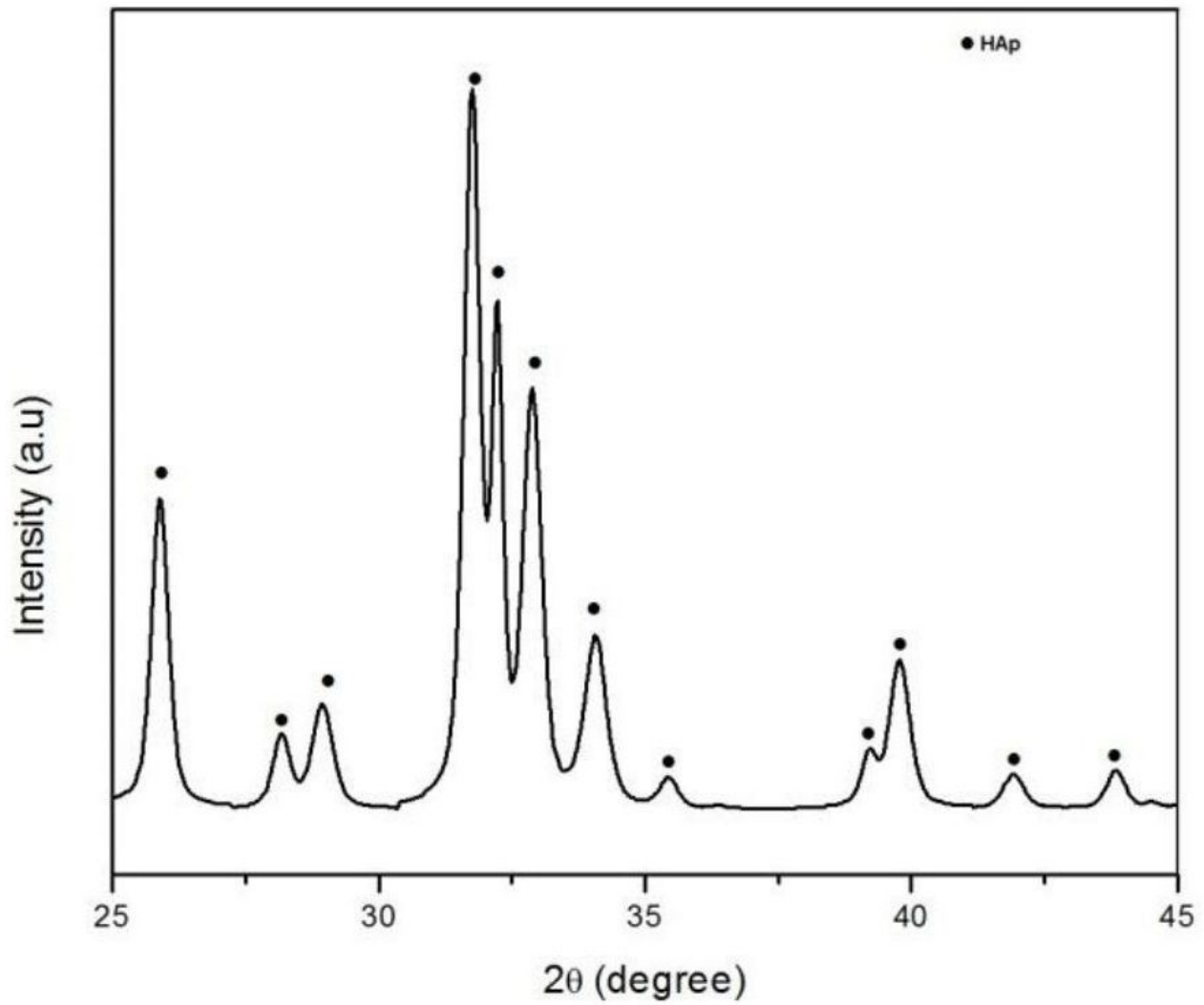


Figure 1

XRD pattern of pure HAp calcined at 700°C

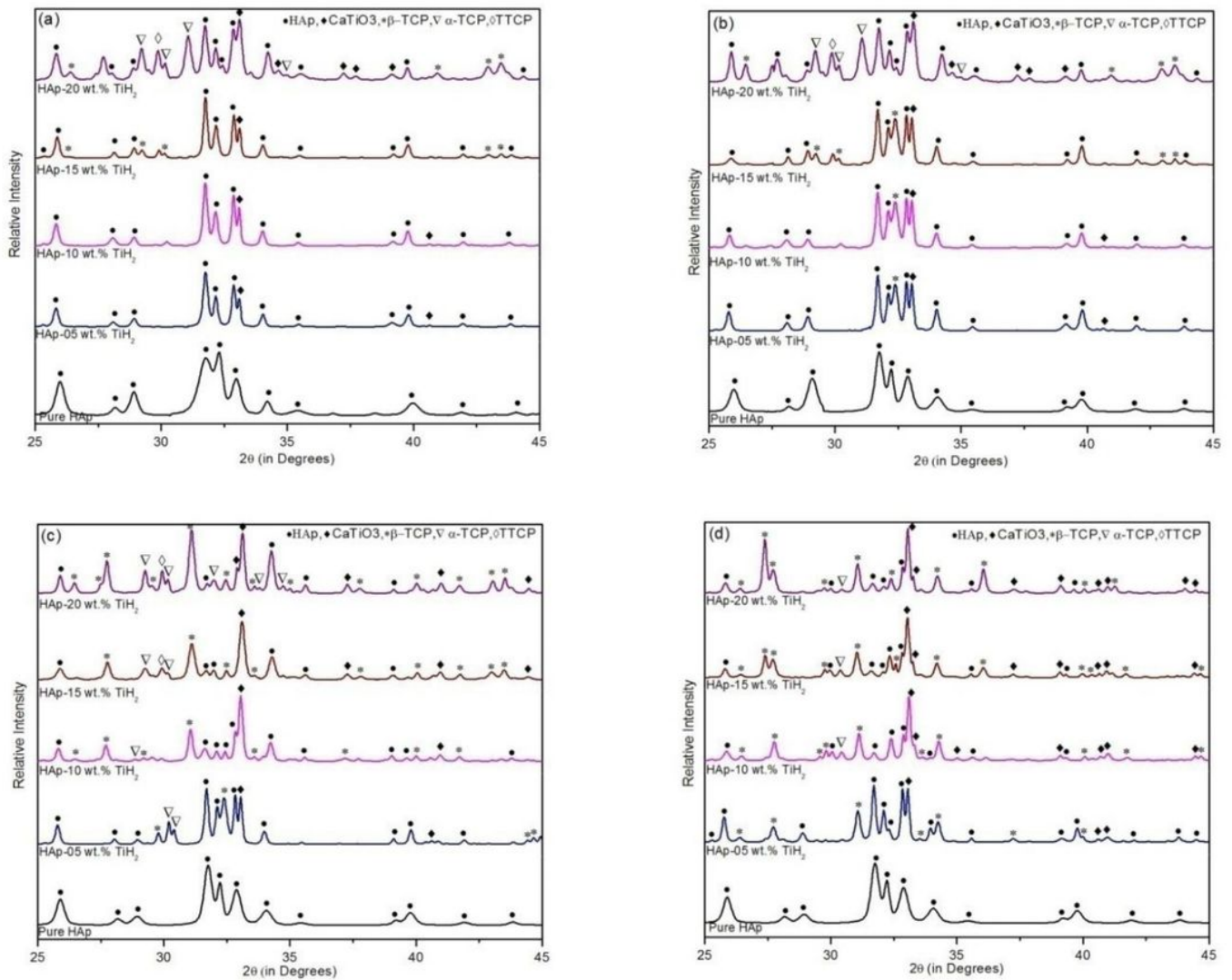


Figure 2

XRD peaks obtained after sintering at temperatures of (a) 900°C (b) 1000°C (c) 1100°C and (d) 1200°C for HAp with different TiH_2 contents

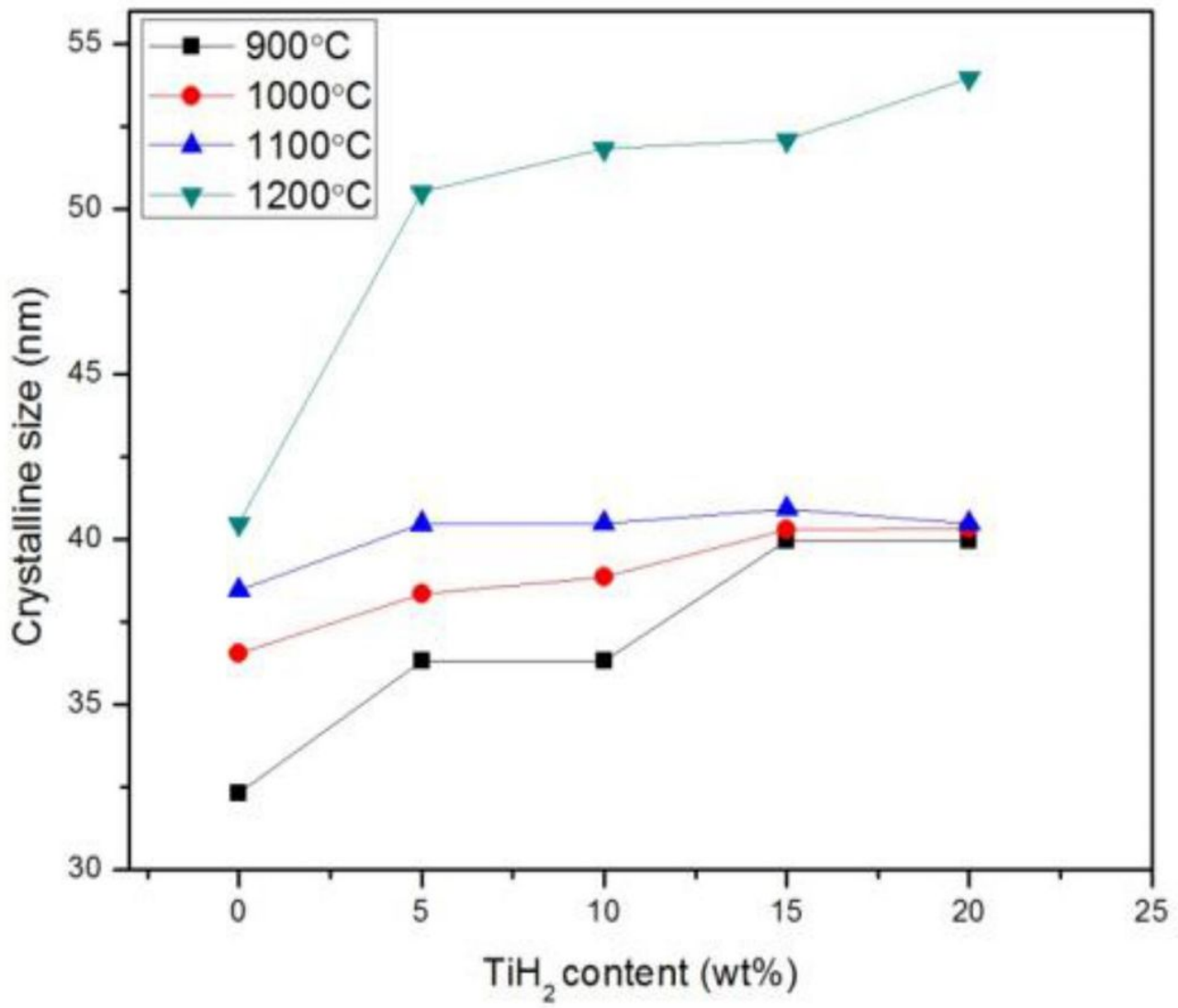


Figure 3

Plot of the crystallite size vs. TiH₂ content at various temperatures

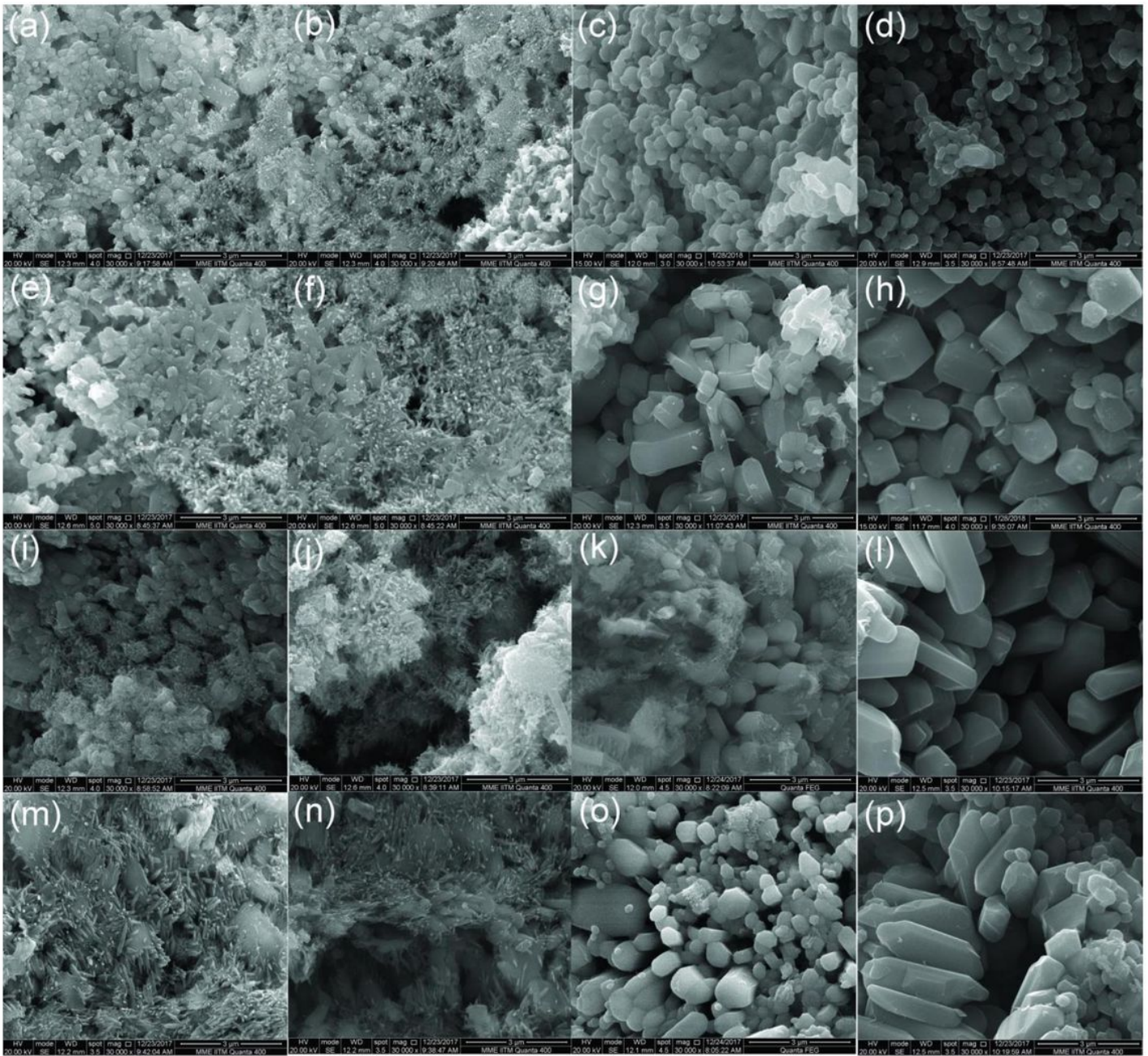


Figure 4

SEM micrographs showing different morphological characteristics: (a), (e), (i) and (m) HAp-5%,10%,15% and 20% TiH₂ sintered at 900°C; (b) (f), (j) and (n) HAp-5%,10%,15% and 20% TiH₂ sintered at 1000°C; (c) (g), (k) and (o) HAp-5%,10%,15% and 20% TiH₂ sintered at 1100°C, (d) (h), (l) and (p) HAp-5%,10%,15% and 20% TiH₂ sintered at 1200°C.

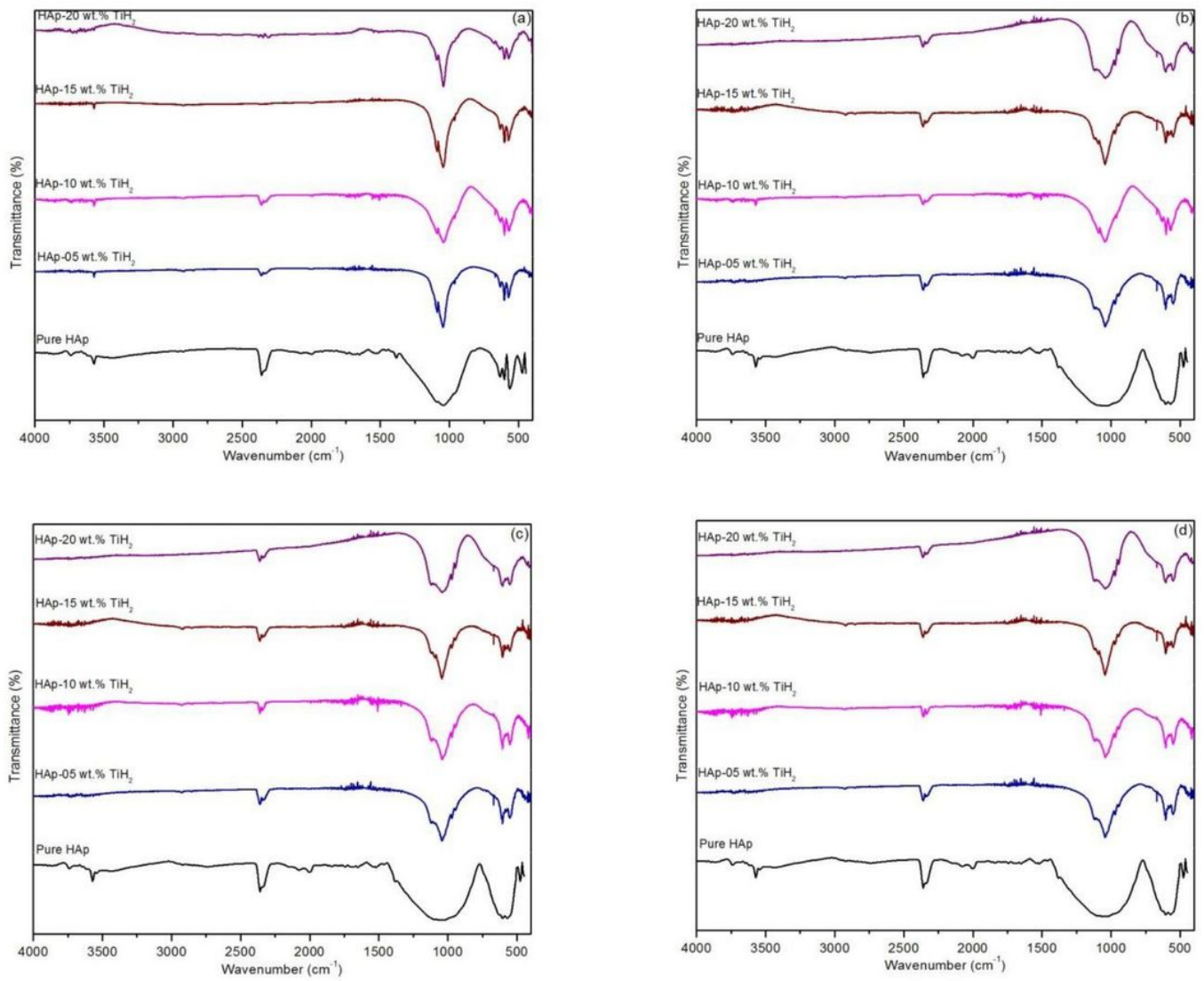


Figure 5

FT-IR spectra obtained after sintering at (a) 900°C, (b) 1000°C, (c) 1100°C and (d) 1200°C from various HAp-TiH₂ composites

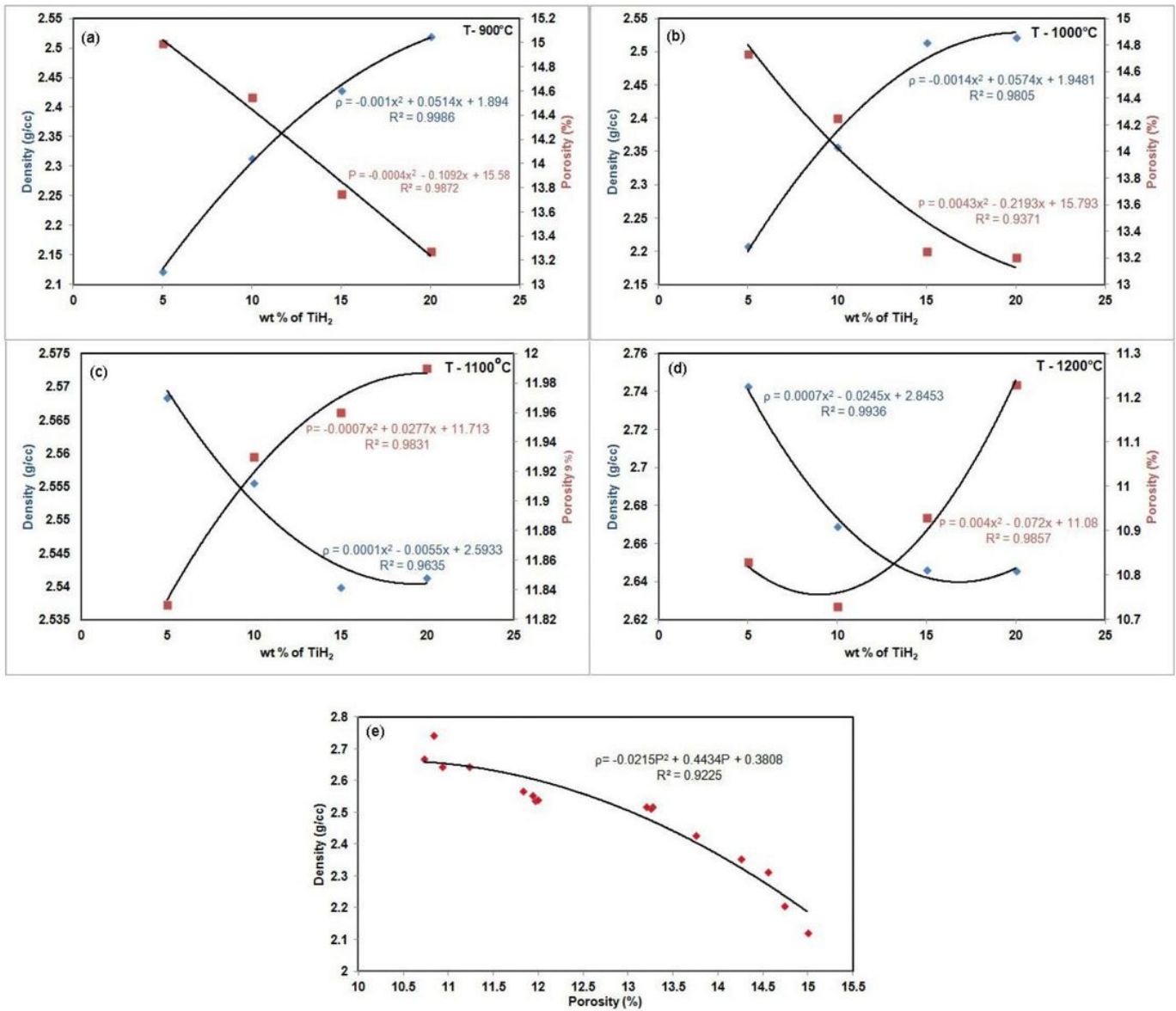


Figure 6

Density and porosity graph of HAp with different weight percentages of TiH₂ (a) sintered at 900°C (b) sintered at 1000°C (c) sintered at 1100°C(d) sintered at 1200°C(e) Overall graph of density vs porosity.